International Journal of Machine Tools & Manufacture 49 (2009) 599–612

Contents lists available at ScienceDirect

International Journal of Machine Tools & Manufacture

journal homepage: www.elsevier.com/locate/ijmactool

Analyzing the performance of diamond-coated micro end mills

C.D. Torres [a], P.J. Heaney [b], A.V. Sumant [c], M.A. Hamilton [d], R.W. Carpick [d], F.E. Pfefferkorn [a,*]

[a] Department of Mechanical Engineering, University of Wisconsin-Madison, 1513 University Avenue, Madison, WI 53706, USA
[b] Material Science Program, University of Wisconsin-Madison, USA
[c] Center for Nanoscale Materials, Argonne National Laboratory, USA
[d] Department of Mechanical Engineering & Applied Mechanics, University of Pennsylvania, USA

ARTICLE INFO

Article history:
Received 18 September 2008
Received in revised form
4 February 2009
Accepted 8 February 2009
Available online 20 February 2009

Keywords:
Micro end milling
Nanocrystalline diamond (NCD)
Fine-grained diamond (FGD)
Coating
Friction
Hot-filament chemical vapor deposition (HF-CVD)

ABSTRACT

A method is presented to improve the tool life and cutting performance of 300 μm diameter tungsten carbide (WC) micro end mills by applying thin (<300 nm) fine-grained diamond (FGD) and nanocrystalline diamond (NCD) coatings using the hot-filament chemical vapor deposition (HF-CVD) process. The performance of the diamond-coated tools has been evaluated by comparing their performance in dry slot milling of 6061-T6 aluminum against uncoated WC micro end mills. Tool wear, coating integrity, and chip morphology were characterized using SEM and white light interferometry. The initial test results show a dramatic improvement in the tool integrity (i.e., corners not breaking off), a lower wear rate, no observable adhesion of aluminum to the diamond-coated tool, and a significant reduction in the cutting forces (>50%). Reduction of the cutting forces is attributed to the low friction and adhesion of the diamond coating. However, approximately 80% of the tools coated with the larger FGD coatings failed during testing due to delamination. Additional machining benefits were attained for the NCD films, which was obtained by using a higher nucleation density seeding process for diamond growth. This process allowed for thinner, smaller grained diamond coatings to be deposited on the micro end mills, and enabled continued operation of the tool even after the integrity of the diamond coating had been compromised. As opposed to the FGD-coated end mills, only 40% of the NCD-tools experienced delamination issues.

1. Introduction

Micro-manufacturing is a rapidly growing worldwide industry estimated at $60 billion [1]. This rapid growth is due largely to the increased interest in fabricating micro/meso-scaled components that will bridge the micro- and nano-scaled worlds to the macroworld [2]. However, many of these components require the use of various robust engineering materials, such as steel, aluminum, titanium, ceramics, and composites, to produce rigid, complex three-dimensional shapes [3–5]. Current micro-manufacturing processes, such as lithography, LIGA, plasma etching, etc., lack the ability to produce high aspect ratio three-dimensional shapes and are limited to silicon-compatible materials [3,4]. Due to these limitations, research has turned to the miniaturization of current mechanical manufacturing processes as a method of producing these complex micro-components [1]. Micro-mechanical manufacturing is the process of creating features and components measuring microns in dimension [1,5]. It is used, for example, in the production of small parts such as X-ray lithography masks, micro-scale heat sinks, micro-fluidic devices, the miniaturization of common devices including actuators, motors, fuel cells, and gas turbines, and the production of packaging that links smaller devices, such as MEMS, to the macroscopic world [1,2,5,6]. As technology shrinks and the demand for smaller devices grows, the ability to precisely manufacture new and existing materials at smaller scales becomes increasingly important [1,2,5].

One micro-manufacturing process of growing importance is micro end milling. As the direct scale-down of macroscopic end milling, micro end milling is a material removal process that can generate high aspect ratio, three-dimensional features in a single step [2,5,7]. It is not limited to special clean room environments, and is therefore more affordable and simple to carry out. It is compatible with various engineering materials such as polymers [8], metals and metal alloys [4,8–10], and pre-sintered powder ceramics [11,12]. Two examples of parts fabricated using micro end milling are illustrated in Fig. 1.

There are several important challenges to overcome when scaling down end mills to microscopic sizes. Sintered tungsten carbide with a cobalt binder is brittle and the micro-scaled features of the end mills are easily damaged, resulting in rapid tool degradation. Also, due to their small diameter, micro tools

* Corresponding author. Tel.: +1 608 263 2668; fax: +1 608 265 2316.
E-mail address: pfefferkorn@engr.wisc.edu (F.E. Pfefferkorn).

0890-6955/$ - see front matter © 2009 Elsevier Ltd. All rights reserved.
doi:10.1016/j.ijmachtools.2009.02.001

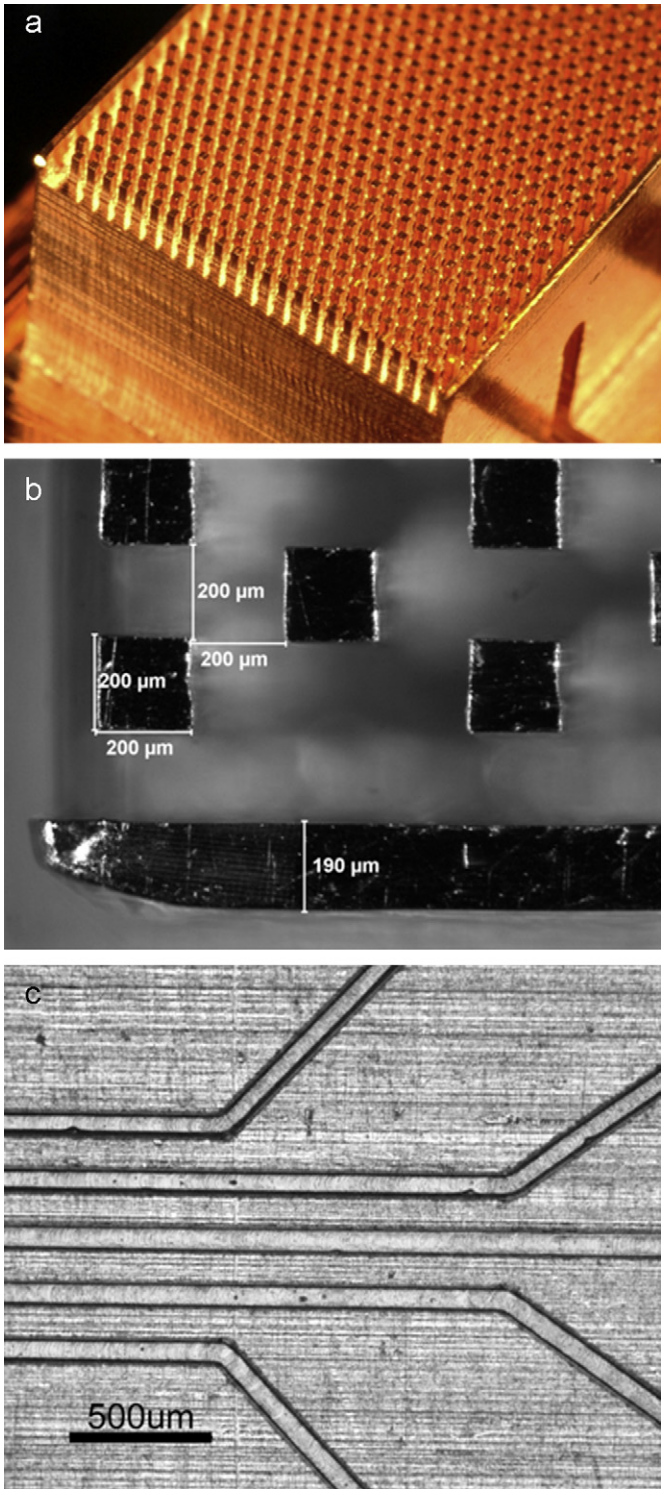

Fig. 1. Fabricated micro-scaled parts: (a) micro pin fin heat sink, (b) heat sink micro pin fin dimensions, and (c) micro-fluidic channels.

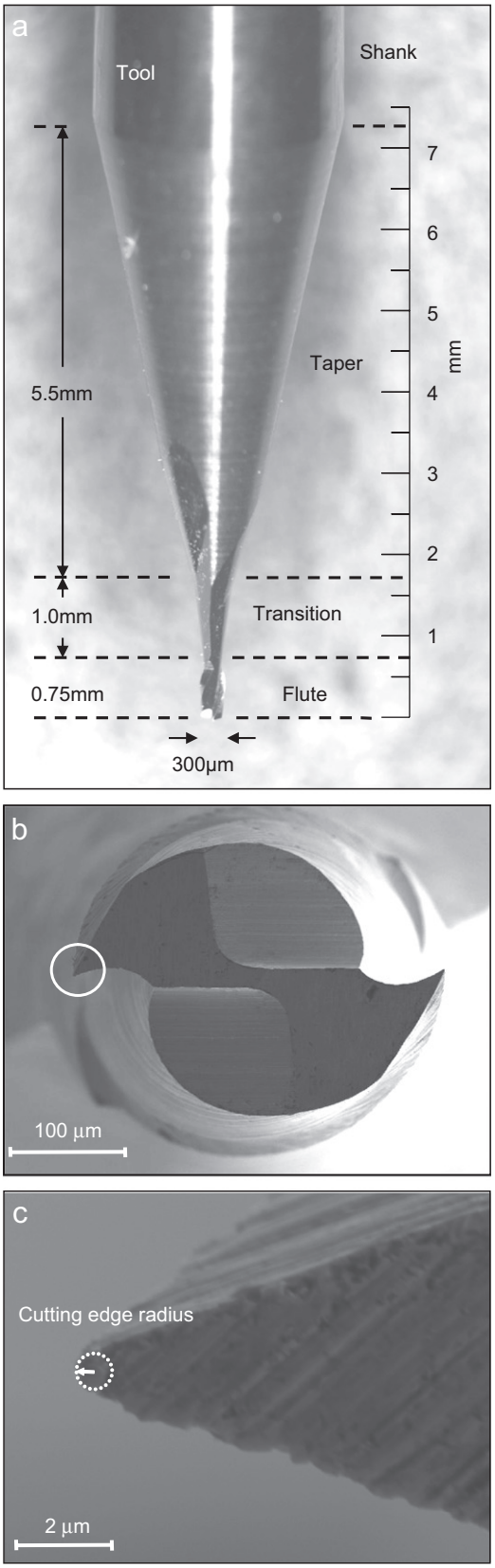

Fig. 2. Micro end mill tool dimensions: (a) optical image showing all sections of the tool, (b) SEM image of the cutting end of the end mill, and (c) SEM image of the cutting tip of the end mill.

have low flexural stiffness and strength [5,7,10]. Relatively small cutting forces can significantly bend the tool, negatively affecting the cutting process and potentially causing catastrophic tool failure [5,7,10]. To avoid this, cutting forces must be maintained below a critical value by ensuring that the uncut chip thickness (i.e., the chip load) remains sufficiently small. For many high-strength materials (e.g., steel, titanium, etc.) the maximum allowable chip load is on the order of or less than the cutting edge radius (the radius of the forward edge of the tool) [10,13], which for typical micro end mills is $<1.5\,\mu m$ (Fig. 2). This can result in material being removed by a rubbing or burnishing process rather than a cutting process, accelerating tool wear and

producing a poor surface finish [5,7]. Also, any chips adhering to the tool will eliminate a path for chips to evacuate the cutting zone and will result in a spike in the cutting forces often leading to catastrophic tool fracture due to the low flexural strength of the tool.

Diamond coatings for micro end mills are promising because of their potential to eliminate many of these limitations currently hindering micro end mill performance and operational life. Previous micro drilling studies using hot-filament chemical vapor deposition (HF-CVD) diamond coatings indicated a threefold increase in the number of acceptable holes drilled in both printed circuit boards (typically a phenolic, glass fiber, and epoxy composite), and aluminum work pieces when compared to an identical uncoated tool [14–16]. These machining improvements are due to many favorable mechanical and tribological properties that diamond coatings possess, such as high hardness, chemical inertness, low adhesion to many materials, and low friction [15,17–21]. The diamond surface has been shown to have an intrinsically low affinity for Al at the atomic scale [22]. The low adhesion of workpiece material helps prevent chips from adhering to the flute surface, hence reducing tool clogging and associated sporadic force spikes [15,17–21]. This, and the low coefficient of friction, reduces the forces exhibited on the cutting tool [15,17–21]. The high hardness reduces the rate of abrasive tool wear [7,15,17–21].

However, the nucleation and growth techniques used for conventional microcrystalline diamond (MCD) coatings for macro-scale cutting tools often require coatings that are too thick ($>2\,\mu m$) for micro tools since thinner films are not continuous. These coatings would significantly increase the $\sim$1.5 μm cutting edge radius, blunting the tool. As it is, the existing cutting edge radius of uncoated tools is larger than desirable, and increasing the cutting edge radius will negatively affect machining performance. MCD films, with grain sizes typically ranging from at least 100 nm up to several micrometers are also too rough for micro tools. In addition, they have inferior strength [23] and much higher friction [24] than nanocrystalline diamond (NCD) films. To take advantage of the best properties, nanocrystalline diamond coatings for micro end mills are investigated here. By achieving high nucleation densities, continuous, thin ($\sim$100 nm) films were reproducibly grown with an average grain size of approximately 50 nm and a measured roughness of 30 nm on 300 μm diameter end mills. This work characterizes the cutting performance of these thin NCD coatings when dry cutting 6061-T6 aluminum.

2. Experimental procedure

2.1. Diamond synthesis

Diamond coatings were synthesized on 300 μm diameter, two-flute, tungsten carbide (WC) end mills with an approximate cutting edge radius of 0.5 μm using HF-CVD. The micro end mills are a commercially available design (Performance Micro Tool, Inc.) and contain 6–8% cobalt (Co) binder located at the WC grain boundaries. Each tool is initially inspected via SEM for defects and is sorted based on the tool diameter. Defect-free tools are then subjected to a three-step nanocrystalline diamond synthesis process: etching, seeding, and diamond synthesis. A hydrofluoric and nitric acid mixture is used to selectively etch cobalt from the surface of the tool since cobalt inhibits the growth of diamond. Diamond nanoparticles are deposited on the tool surface to create nucleation sites for diamond growth using two different methods, described below. The tools are then placed into the HF-CVD vacuum chamber (base pressure 0.10 Torr). A mixture of 4% methane (flow rate 3.75 SCCM) and 96% hydrogen (flow rate 90 SCCM) at a pressure of 30 Torr flows over tungsten filaments at 2000 °C, dissociating the gases which then impinge on the tool and react to synthesize diamond. A detailed description of the synthesis process is presented by Heaney et al. [25].

2.1.1. Seeding

Chemical vapor deposition (CVD) of diamond does not occur easily on non-diamond substrates [15,26–28]; therefore, nano-diamond particles are seeded on the surface to help promote the diamond growth process and control where diamond nucleation occurs. Each of the seeded diamond particles produces a nucleation site for initial diamond growth. Hence, a dense, uniform seeding procedure is ideal for producing thin, conformal coatings. Typically, diamond growth occurs in a columnar fashion [29], requiring extensive diamond growth to occur for complete film coalescence of a poorly seeded surface. The long growth time will often result in large-grained ($\sim$1 μm), thick diamond films ($>1\,\mu m$).

Mirco end mills were seeded using two different diamond seed solutions. The first solution was a mixture of a dry detonation nanodiamond powder (DET) composed of 20–50 nm diameter particles, dissolved in methanol. However, the dry diamond particles often agglomerated, resulting in diamond seeds 60–80 nm in diameter. The tool tips were suspended within the solution and ultrasonically treated to attach the diamond seeds onto the tool surface. This type of seeding method resulted in diamond particle coverage of 7.3% of the tool surface area as determined from SEM images (Fig. 3a). The other diamond solution consisted of ultra-disperse diamond (UDD) nanodiamond particles (25–30 nm) suspended in dimethylsulfoxide and diluted in methanol. Seeding coverage for this method is approximately 59.8% (Fig. 3b). After 15 min of seeding, the tools were ultrasonically rinsed for 10 min in a methanol bath to remove large diamond particle agglomerations from the surface of the tool. Fig. 3 compares the coverage of the two seeding methods on polished silicon samples. The smooth silicon allows for easy visibility of the diamond seeds.

2.1.1.1. Diamond growth with detonation nanodiamond (DET) seeding. The larger diameter, less dense DET diamond seed requires a minimum growth time of 20 min to produce a completely coalesced diamond film. The long growth time is primarily attributed to the low nanoparticle density (Fig. 3a) and thus, a low density of nucleation sites. The low nucleation site density required extensive diamond deposition to occur before the diamond grains began to coalesce and form a continuous film. Fig. 4 contrasts the amount of growth required before film coalescence for low- and high-density seeding. This growth time resulted in a minimum coating thickness of approximately 600 nm, with most coatings being approximately 1 μm thick for complete coalescence. The long growth time resulted in a fine-grained diamond (FGD) coating with grains measuring between 500 and 1000 nm (Fig. 5c).

Typical DET-seeded diamond-coated tools experience an increase in the cutting edge radius of approximately 120% (measured via SEM), which results in an overall cutting edge radius of approximately 1.2 μm. Generally, tools that experience significant blunting from diamond coating have broken immediately on contact during machining. Fig. 5 illustrates the difference in cutting edge radius between an uncoated and FGD-coated end mill, along with the overall coating thickness.

2.1.1.2. Diamond growth with ultra-disperse diamond (UDD). The high seeding density of UDD-seeded diamond (Fig. 3b) requires a growth time of 5 min to achieve a completely coalesced coating.

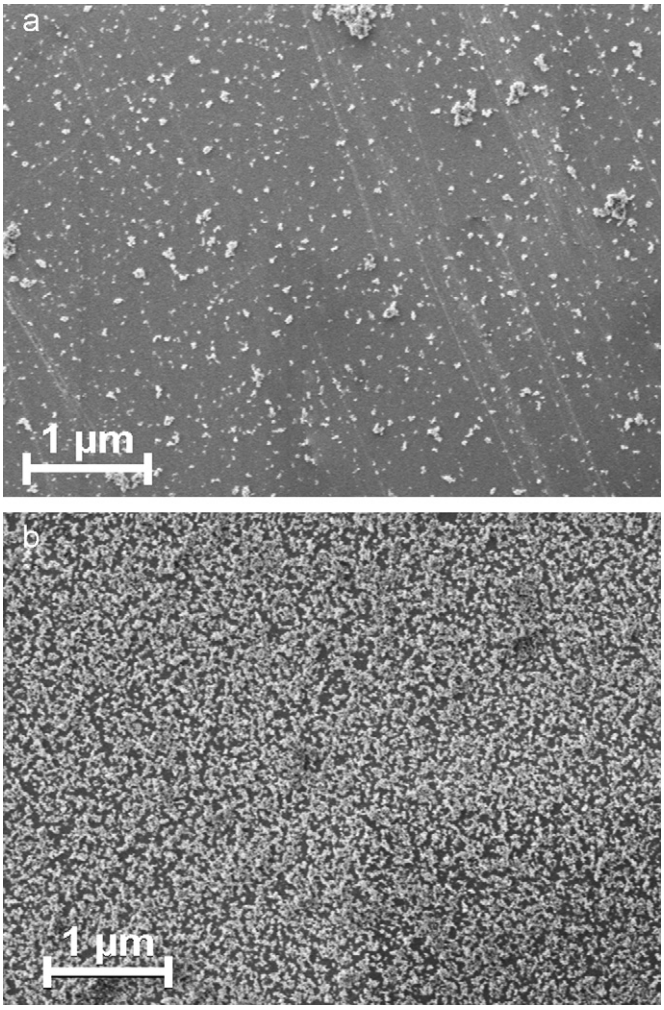

Fig. 3. SEM images of diamond seed density on silicon samples for (a) DET diamond seed and (b) UDD diamond seed.

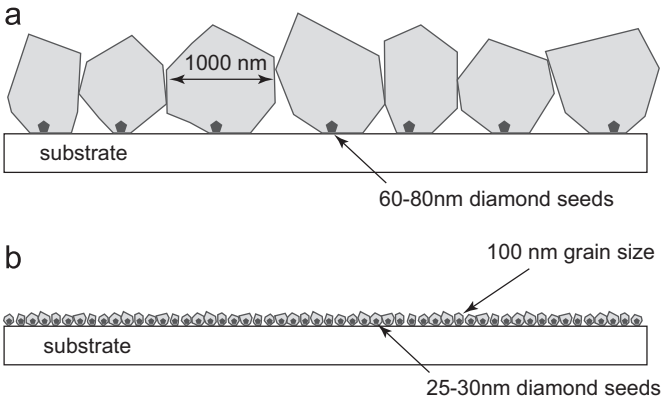

Fig. 4. Comparison of diamond growth for (a) low nucleation density and (b) high nucleation density.

Coatings as thin as 110 nm have been grown with typical coatings consistently being grown between 200 and 300 nm thick with NCD grain sizes <100 nm (Fig. 6a). Unlike conventional MCD diamond coatings, these thin coatings do not drastically alter the cutting edge radius of the end mills (Fig. 6b). The typical cutting edge radius of UDD-seeded NCD-coated tools is approximately

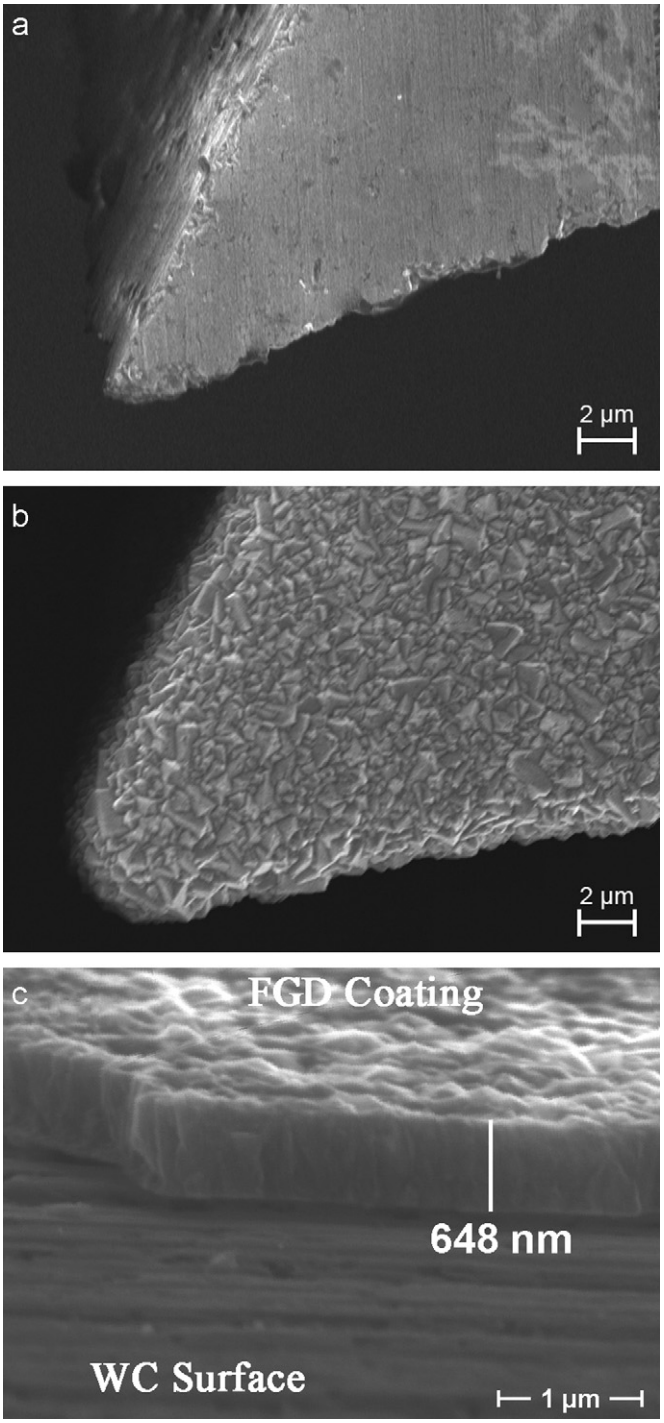

Fig. 5. SEM micrographs of unused micro end mill cutting tips: (a) uncoated tool, (b) FGD-coated tool, and (c) FGD coating thickness.

850 nm, which is approximately a 54% increase (measured via SEM) over the as-ground edge.

2.2. Diamond characterization

Due to the nature and complexity of the CVD diamond process, film growth is very sensitive to any deviations in growth conditions. Small changes in temperatures or gas chemistry will often result in significantly different diamond structures and bonding characteristics of the diamond film. It is important to characterize each coating before testing it on the end mills. A Leo

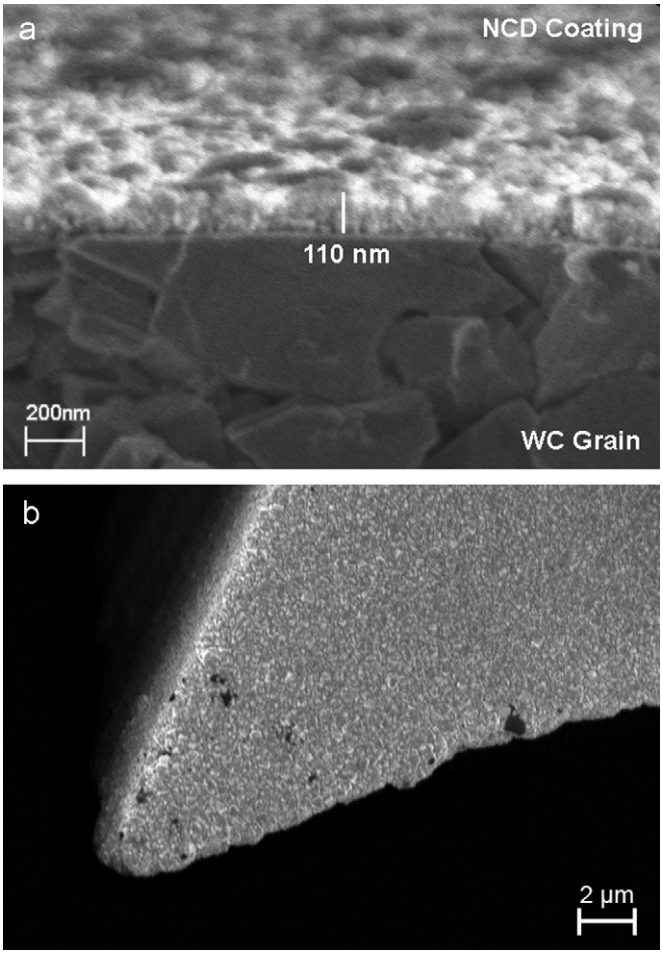

Fig. 6. SEM images of diamond coating after UDD-seeding: (a) thickness and (b) on micro end mill cutting tip.

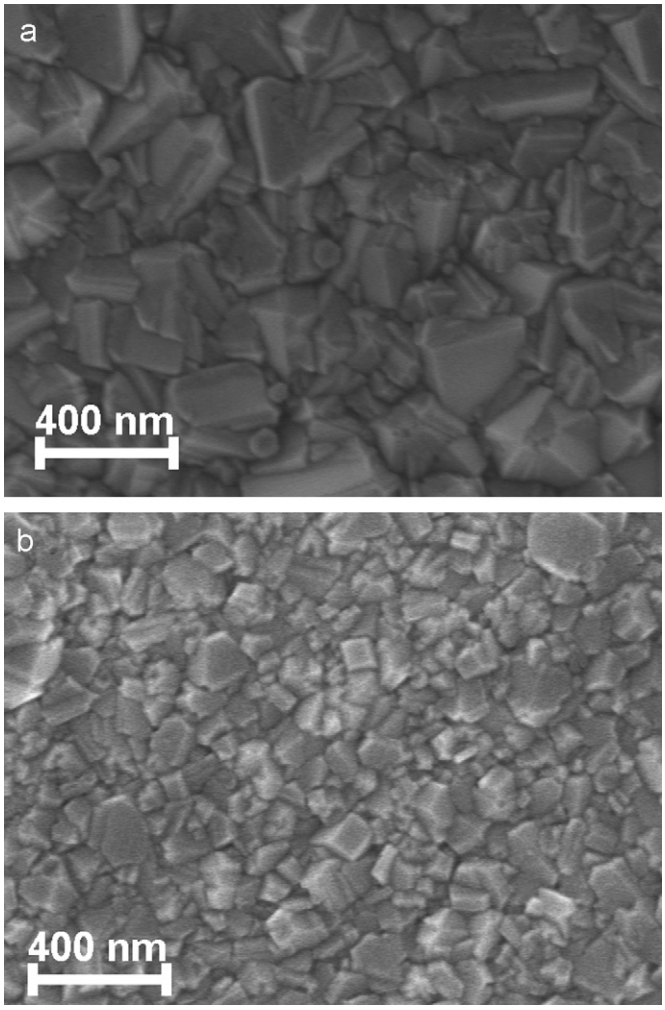

Fig. 7. SEM images of apparent diamond grain sizes for (a) ~600 nm thick FGD coating and (b) ~200 nm thick NCD coating.

1530 field emission scanning electron microscope (SEM) is used for visual inspection of each of the diamond films to estimate both the grain size of the film and the film thickness via changes in the cutting edge radius of the tools. In addition, the SEM is used to verify the uniformity and coalescence of the diamond films on the tool surface. The roughness of the tools, both before and after coating, is measured using a white light profilometer (Zygo NewView 6400) and locally measured using an atomic force microscope (AFM, Ambios Technology QScope 250).

2.2.1. Grain size

The grain size of diamond coatings was qualitatively estimated using SEM. The lower nucleation density and longer growth time of the DET diamond seeding result in larger diamond grains at the surface, 500–1000 nm, while the UDD diamond seeding consistently produces diamond grains <100 nm (Fig. 7). Nanocrystalline diamond is defined as having grains between 10 and 100 nm in size. In a conventional columnar growth process since the grain size is dictated by initial nucleation density, the DET-seeding method produces fine-grained diamond coating (grain size between 100 and 1000 nm) as seen in Fig. 5(c) [25]. However, the UDD-seeding method does produce an NCD coating.

2.2.2. Roughness

The surface roughness of the tool is measured macroscopically within a 50 μm × 50 μm area using the white light profilometer, while the local roughness is measured within a 10 μm × 10 μm and a 1 μm × 1 μm area using an AFM. The macroscopic roughness measurements are dominated by the features formed in the tool surface during the grinding process. The local roughness measurements are sensitive to the surface texture of the diamond coatings by effectively filtering out the longer wavelength features created by grinding. The direction used in grinding the tool shape is very apparent within these measurements and results in an average surface roughness of Ra = 207 nm, a root-mean-square roughness of Rq = 274 nm, and an average peak spacing of Sm = 6.46 μm. These are low spatial frequency features that can dominate the surface texture and apparent friction when only thick coatings are applied.

On the other hand, the local roughness (high spatial frequency) measurement by AFM is much more sensitive to the surface

Table 1
Summary of diamond coating roughness measurements.

Coating classification	FGD		NCD	
Seeding	DET		UDD	
Thickness	>600 nm		100–300 nm	
Grain size	500–1000 nm		20–100 nm	
Surface roughness	Ra (nm)	Rq (nm)	Ra (nm)	Rq (nm)
White light interferometer 50 μm × 50 μm	207	274	199	244
AFM 10 μm × 10 μm	44	56.5	30.4	38.7
AFM 1 μm × 1 μm	27.4	32.5	17.6	22.2

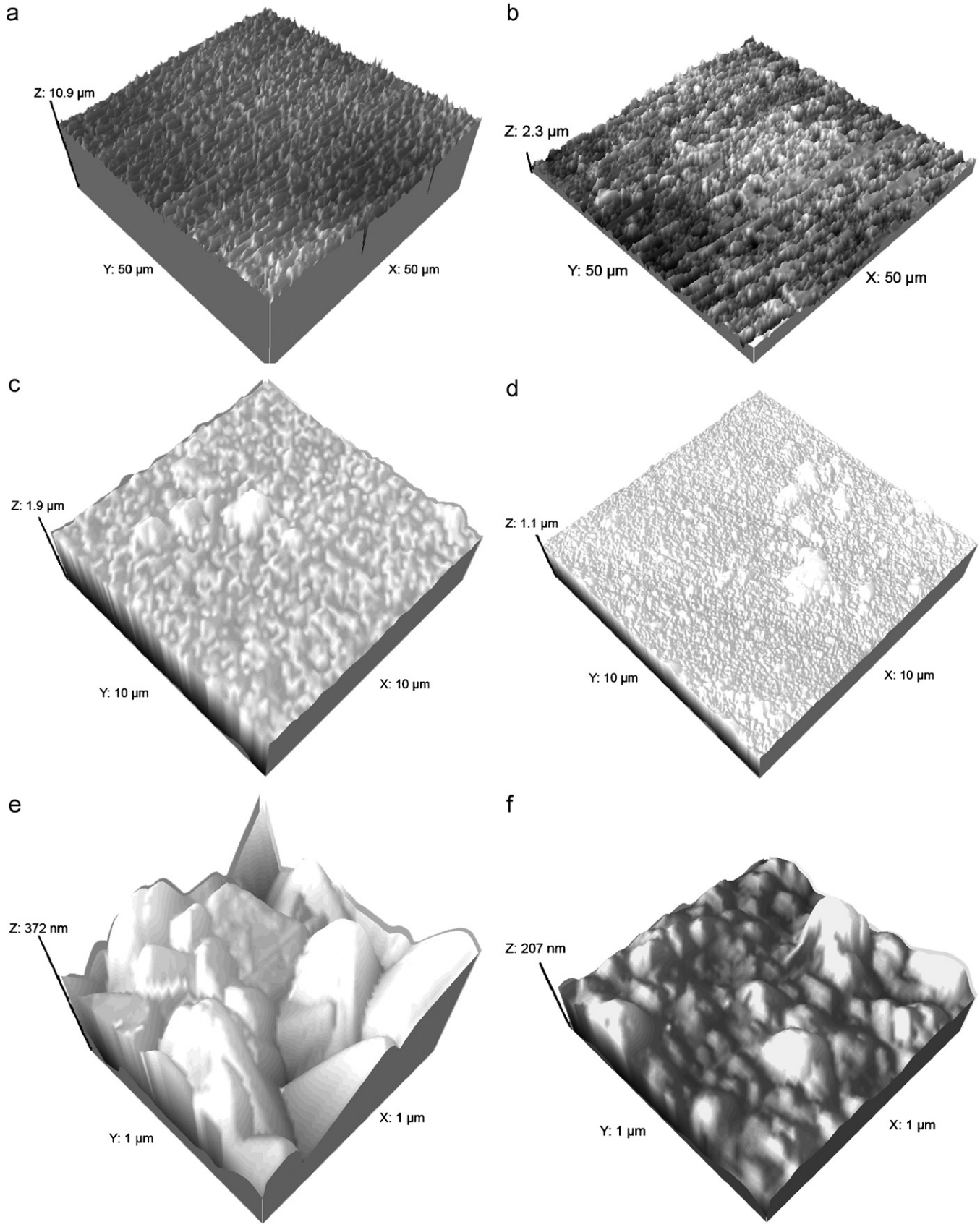

Fig. 8. Three-dimensional topography view of a representative FGD coating (left) and NCD coating (right). (a,b) 50 µm × 50 µm white light interfermetric scan, (c,d) 10 µm × 10 µm AFM scan, and (e,f) 1 µm × 1 µm AFM scan.

texture created by the diamond facets, causing roughness on this scale to be highly sensitive to the growth conditions used for the diamond coating. Table 1 summarizes the Ra and Rq roughness values of the diamond coatings measured with a 1 μm × 1 μm and a 10 μm × 10 μm scan size.

The difference in roughness between the two samples is directly related to the diamond grain size (Fig. 8), which is a result of the differences in growth time and nucleation density.

Initial tribology tests have shown that the roughness on both scales can significantly affect the friction experienced between the cutting tool surface and workpiece. As discussed later on within the paper, higher friction can significantly alter the performance and cutting forces of the end mills.

2.3. Micro end milling tests

2.3.1. Apparatus

Fig. 9 illustrates the test setup used for the machining experiments. A high-speed spindle (NSK-HES500) with electric drive and ceramic bearings was mounted onto the spindle of a CNC milling machine (HAAS TM-1). The high-speed spindle (5000–50,000 rpm) was nominally operated at 40,000 rpm for all of the experiments. A fixed tool feed rate of 500 mm/min was used throughout the experiments. This feed rate, coupled with the spindle rotational speed, resulted in a maximum chip load applied to the cutting tool of 6.25 μm/tooth.

Forces acting on the 6061-T6 aluminum workpiece were measured by a three-axis force dynamometer (Kistler 9256C2). The dynamometer was able to dynamically measure the cutting forces in the *x*, *y*, and *z* axes. However, the forcing frequency of a two-flute end mill rotating at 40,000 rpm, 1.3 kHz, was close enough to the 4 kHz natural frequency of the dynamometer to create an indeterminate bias associated with the measured cutting forces. Therefore, workpieces of identical mass were used throughout the tests thus allowing data between different cutting conditions to be comparable. A humidity control system was used to maintain a constant relative humidity of approximately 85% at the tool–workpiece interface.

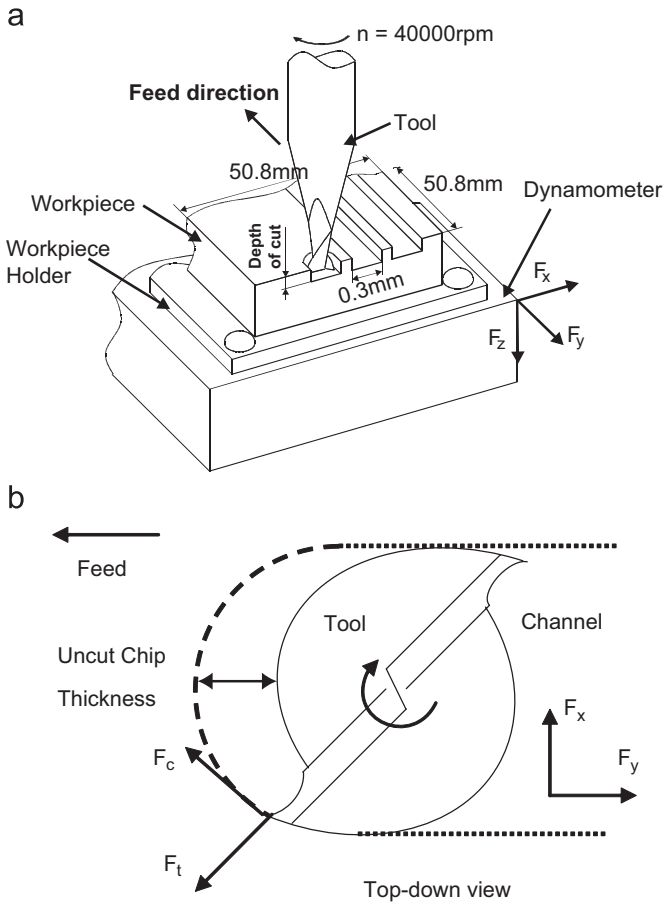

Fig. 9. Schematic of micro end milling: (a) three-dimensional view of the experimental setup and (b) end view of the cutting process.

Table 2
Machining conditions.

Workpiece material	6061-T6 aluminum
Room temperature	~23 °C
Relative humidity	~85%
Tool (end mill)	
Material	0.4 μm grain carbide
Diameter	304.8μm (0.012 in)
Flutes	2
Helix	30°
Spindle speed	40,000 ± 500 rpm
Feed rate	500 mm/min
Feed	12.5 μm/rev
Chip load	6.25 μm/tooth
Depth of cut	100 ± 10 μm
Coolant	None

2.3.2. Cutting conditions

The machining conditions used are shown in Table 2. The tests consisted of dry machining a single full-width channel 5 mm long and 100 μm deep, in a 50 mm × 50 mm × 4.8 mm 6061-T6 aluminum block. The workpiece was mounted on the dynamometer before preparing the surface. The workpiece surface was prepared by facing with a 1 in end mill to ensure flatness within 3 μm. Each tool was fixtured in the high-speed spindle and then aligned to the workpiece using an optical magnification system. The alignment uncertainty was ±10 μm in the *z*-axis, which corresponds to an uncertainty in the depth of cut. LabView software and National Instruments data acquisition hardware (NI PCI 6014) were used to record the force data at a rate of 60 kHz. Both uncoated and coated tools were run in the same test batch to ensure compatibility between tests.

2.3.3. Force data analysis

Tool cutting and thrust forces were calculated based on the measured global *x* and *y* force. Although the force in the *z*-direction had been collected, it is largely ignored during the force conversion calculations since orthogonal cutting was assumed throughout the analysis. In order to properly convert the global *x* and *y* force data into cutting and thrust force, the rotational angle of the tool, θ, must be determined. The rotational angle of the tool with respect to the workpiece was determined directly from analysis of the raw F_x and F_y data. A tool angle of 0° was defined as the instantaneous point that the tool tip comes in contact with the workpiece. At that point, the force in the *x*-direction will be zero, while the *y*-direction force will be at a negative maximum. Using the raw data, a 90° tool angle was first determined by locating the maximum F_x. The data was then fit with a sinusoidal wave function, with the 0° tool angle located by interpolation from the 90° tool angle point.

Using the raw F_x and F_y data and the tool angle θ, the global forces can be converted into cutting and thrust forces using the equations:

$$F_c = F_x \sin\theta - F_y \cos\theta \quad (1)$$

$$F_t = -F_x \cos\theta - F_y \sin\theta \quad (2)$$

However, the two-flute end mill design restricted the use of these equations for $0^\circ < \theta < 180^\circ$. In order to properly take into account both cutting edges during the cutting and thrust force calculation, the tool rotation angle was reset back to 0 after 180° of rotation. In addition, the limitations imposed on the frequency of data collection often result in an ill-defined 0° tool rotational point. This limitation, along with uncertainties experienced throughout the machining operation (e.g., spindle speed, depth of cut), can often lead to uncertainties of approximately 10% and 40% in the cutting and thrust forces, respectively, during the force conversion.

3. Results and discussion

3.1. Reduction of cutting and thrust forces

Analysis of the cutting and thrust force data shows a considerable improvement in the amount of force required to mill 6061-T6 aluminum between an uncoated, a thick fine-grained diamond (0.1–1 μm grain size, 0.5–1 μm thick) coated, and an NCD diamond (20–50 nm grain size, 200 nm thick) coated tool. For a 6.25 μm chip load, the main cutting and thrust forces are reduced from 2.14 ± 0.85 N and 4.40 ± 0.44 N to 0.49 ± 0.09 N and 0.34 ± 0.04 N, respectively, when adding an FGD coating to WC tools. Even smaller cutting forces are measured for thin (~200 nm) NCD-coated cutting tools. The NCD coatings further reduce the cutting and thrust forces to 0.18 ± 0.07 N and 0.17 ± 0.02 N, respectively (Fig. 10). In addition to an overall reduction in forces, the cutting and thrust forces measured for the diamond-coated tools are more balanced, while the uncoated tools exhibited a thrust force that is twice the cutting force. This balance in forces indicated a more ideal cutting process with minimal plowing, burring, or adhesion of the chips to the flutes. In addition, the lower forces for diamond-coated tools mean that the specific cutting energy is lower. This has two consequences. First, the machining temperatures of the tool and workpiece at the cutting interface should be lower compared to the uncoated WC tools, resulting in a reduced tool wear rate and adhesion of aluminum. Second, less energy is required for the plastic deformation during chip formation, resulting in a larger shear angle and thus smaller chip thicknesses.

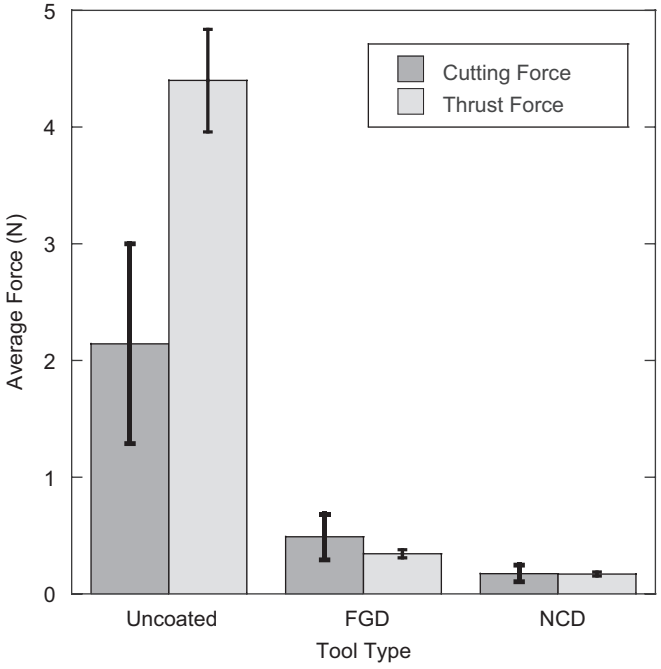

Fig. 10. Cutting and thrust force comparison between an uncoated, a fine-grained diamond coated, and a nanocrystalline diamond-coated end mills.

3.2. Force analysis

Analyzing the tool forces using a simplified, two-dimensional orthogonal cutting model indicated a reduction in friction coefficient and friction force, an increase in shear angle of the primary deformation zone, and reduction in cut chip thickness when using a diamond coating on the cutting tools. The friction force and normal force on the rake face can be determined directly through conversion of the cutting and thrust force using the tool rake angle, γ_{ne}, of 11° [30,31]:

$$F_f = F_c \sin(\gamma_{ne}) + F_t \cos(\gamma_{ne}) \quad (3)$$

$$F_N = F_c \cos(\gamma_{ne}) - F_t \sin(\gamma_{ne}) \quad (4)$$

The friction coefficient for the cutting process was determined by taking the ratio of the frictional force to the normal force [30,31]:

$$\mu = \frac{F_f}{F_N} \quad (5)$$

Analysis of the frictional forces for each of the cutting tools reveals a large friction role on the overall cutting forces. NCD coatings grown on optically smooth surfaces typically exhibit a low friction coefficient of approximately 0.1 [32]. This low coefficient of friction drastically reduces the frictional force the chip experiences when sliding on the tool face. In addition, the chemical inertness of diamond coatings results in very little adhesion of the aluminum workpiece to the cutting tool surface. The lower frictional force and absence of workpiece adhesion directly result in lower cutting and thrust forces required for both chip formation and removal.

The shear angle, φ, can also be calculated using the simplified, two-dimensional orthogonal model using both the workpiece material properties and the measured cutting forces using the equation [30,31]

$$\sigma = F_c \sin(\varphi) + F_t \cos(\varphi) \frac{\sin(\varphi)}{a_c a_p} \quad (6)$$

where σ is the yield strength of aluminum, 270 MPa, F_c and F_t are the cutting and thrust forces, respectively, a_c is the chip load, 6.25 μm, and a_p is the tool depth of cut, 100 μm. The length of the shear plane and the cut chip thickness, t_c, can be calculated from the shear angle and tool rake angle, γ_{ne} [30,31]:

$$l = \frac{a_c}{\sin(\varphi)} \quad (7)$$

$$t_c = l \cos(\varphi - \gamma_{ne}) \quad (8)$$

Comparing shear angles and chip sizes reveals a large discrepancy between the coated and uncoated tools. The high, unbalanced forces of the uncoated tools result in a small calculated shear angle of about 1.1° and a chip thickness of 164 μm. On the other hand, the lower forces of the NCD-coated tools result in a larger shear angle of 22° and a chip thickness of 8.2 μm.

3.3. Chip formation

Further examination of the chips, end mills, and workpiece verifies these calculations. It must be noted that upon

examination, very little difference was noted between the FGD-coated end mills and NCD-coated end mills in terms of produced surface finish, cut chips, and the overall structural condition of the end mill after machining. Therefore, the observed comparisons will be based on uncoated and diamond-coated tools. The uncoated tools produced larger continuous chips of various sizes (Fig. 11b), while the diamond-coated tools produced more uniform segmented chips. The continuous chips are unusual for an interrupted cutting process such as end milling because a cutting edge is only engaged with the workpiece for 180° of rotation. It is believed that the continuous chips are generated by the uncoated tool because a newly generated chip adheres to the flute surface and is only moved after a newly generated chip is pushed into it, welding them together. This mechanism results in higher thrust forces because a chip that is being created in the primary shear zone must also dislodge a chip adhering to the flute that was generated on the previous tool rotation.

Measurement of the chip thicknesses supports the orthogonal cutting analysis performed. Representative chips produced from the NCD-coated tools are shown in Fig. 11. From the image, the chips have an approximate thickness of 9.3 μm (Fig. 11a), slightly larger than the 8.2 μm thick chips estimated by the model. The error in calculated chip size can be attributed to the assumptions made in the model, which include the cutting edge of the tool being only two-dimensional and perfectly sharp. However, the cut chip thickness of the uncoated tool is drastically smaller than the calculated chip thickness. The measured chip thickness of a representative chip produced with an uncoated tool is approximately 50 μm (Fig. 11b), or approximately three times smaller than the calculated value of 164 μm. This difference can largely be attributed to workpiece adhesion, smearing, and burring that occur during the cutting operation. All of these effects are not taken into account within the two-dimensional orthogonal cutting model, where it is assumed that all of the material is cut and removed from the cutting region as a single chip.

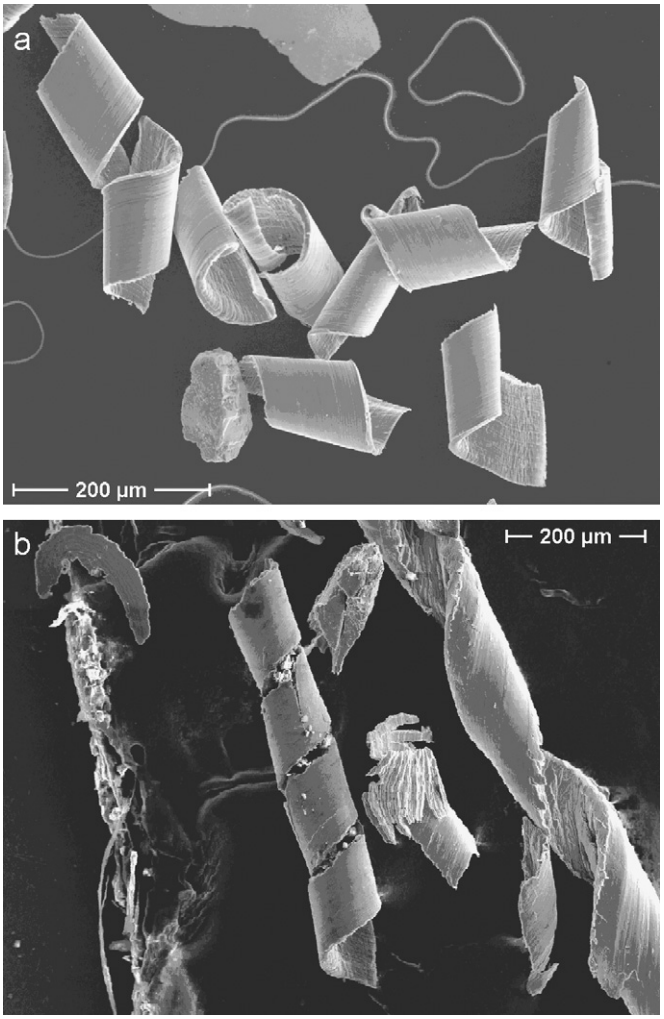

Fig. 11. Comparison of chips generated using (a) an NCD-coated end mill and (b) an uncoated end mill.

3.4. Tool and workpiece comparison

Further inspection of the end mills via SEM and energy-dispersive X-ray spectroscopy (EDS) reveals large portions of adherent aluminum on the cutting edges of the uncoated end mills, leading to a significant built-up edge and possible clogging of the flute. This directly results in larger cutting forces as it becomes much more difficult for the tool to engage the workpiece and proceed with the chip formation. In addition, flute clogging requires higher forces to evacuate the chips from the cutting zone. In several instances, these uncoated tools exhibit either complete tool fracture or partial fracture of a cutting flute as shown in Fig. 12a. The diamond-coated tools, on the other hand, did not exhibit any of these problems. The diamond-coated tools are free of significant aluminum workpiece adhesion, and are structurally sound after machining (Fig. 12b). They display no evidence of tool fracture on either the tool cutting edge or flank edge.

Workpiece examination is consistent with the results gathered from the examination of the end mills. Milled channels were

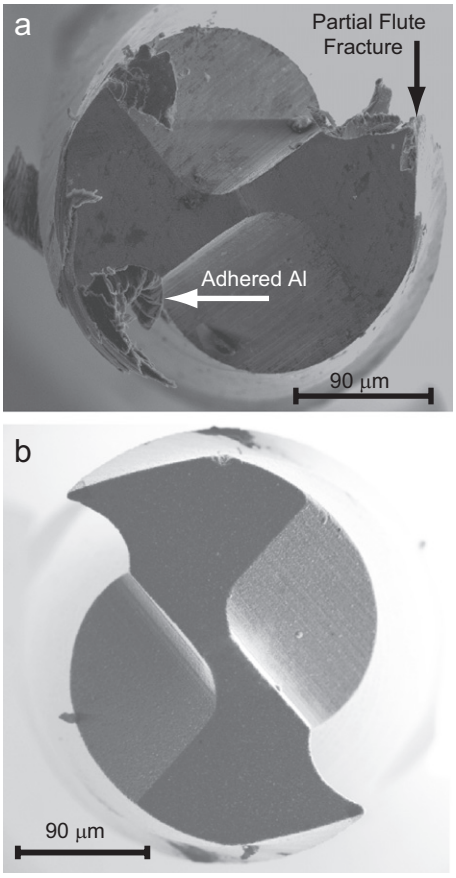

Fig. 12. SEM images representative of tool condition after machining: (a) uncoated tool showing adhesion of Al and partial tool fracture and (b) diamond-coated tool showing no observable adhesion of Al or tool wear.

imaged and inspected using a white light interferometer. Comparing a representative diamond-coated and uncoated channel (Fig. 13) revealed several drastic differences in the surface finish of the channels. Primarily, the channels created by a diamond-coated cutting tool exhibit a highly patterned, uniform bottom surface, while the uncoated tool produced a sporadic surface finish. The non-uniform surface finish of the uncoated tool channels suggests a significant amount of heat generated during the cutting process, resulting in adherent workpiece material on the tool surface. This adherent material often resulted in material smearing and rubbing across the bottom of the workpiece. Further analysis of the channels revealed that the diamond-coated tool produced a smoother channel than the uncoated tool. For the uncoated tool Ra = 350 nm and Rq = 450 nm, whereas for the diamond-coated tool Ra = 325 nm and Rq = 400 nm. Cutting marks can be seen in the channel machined with the uncoated tool (Fig. 13a), although these marks appear to have been smeared out compared with the features generated by the coated tool (Fig. 13b). The coated tool cut much cleaner and left a standard, repeatable surface finish in all channels. In contrast, the surface finish produced by the uncoated tools varied within a single channel and between subsequent cuts (i.e., channels).

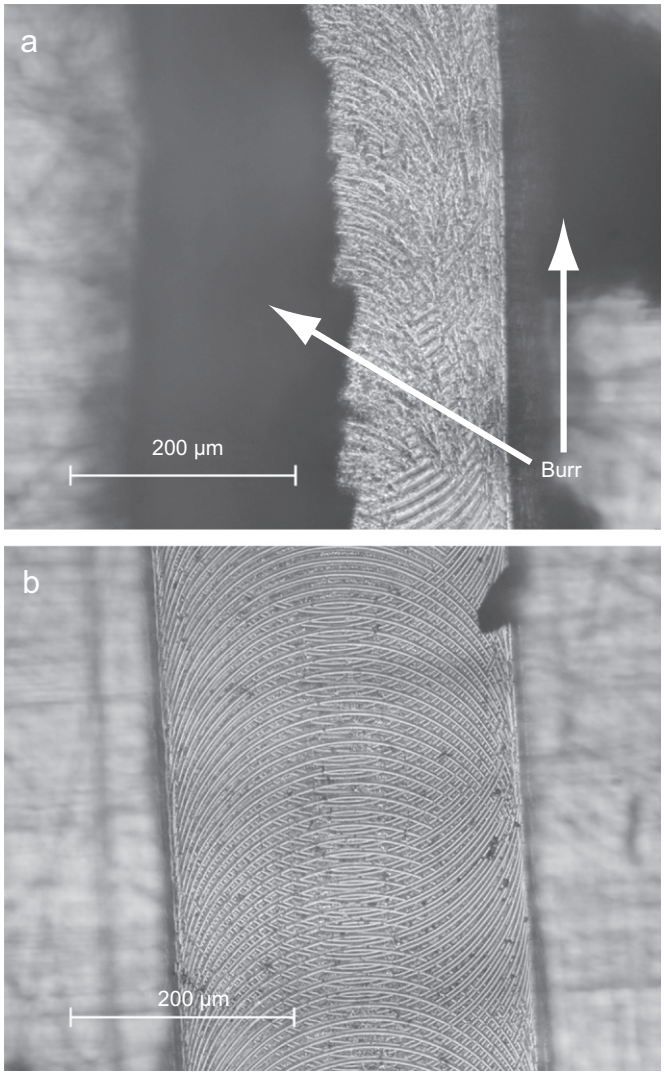

Fig. 13. Optical images of representative end milled channels in 6061-T6 aluminum using (a) uncoated end mill and (b) diamond-coated end mill.

Further inspection of the channel surface finish reveals distinct cutting patterns indicative of the tool stress state. The surface finish of the diamond-coated tool contains a very periodic pattern of concave and convex features, with respect to the cutting direction, throughout the entire channel. This indicates that both the advancing and the retreating cutting edges are in contact with the workpiece throughout an entire tool revolution. The uncoated tool surface finish contains very few convex features, suggesting that the retreating cutting edge is not in contact with the workpiece surface. The higher forces and workpiece adhesion associated with the uncoated tools produce a deflection of the end mill, resulting in liftoff of the retreating cutting edge (Fig. 14).

The deflection is also apparent in the raw force data collected during the cutting operation. The force data for the diamond-coated tools contain highly symmetrical force data centered approximately around 0 N (Fig. 15a). The uncoated tool forces, however, are offset by a few newtons. Fig. 15b illustrates this force bias using representative force data of an uncoated tool, in which the *x*-directional force (Fig. 9) is offset by approximately 1 N and the *y*-directional force is offset by approximately −3 N. Reevaluation of the cutting process in Fig. 15b illustrates that a negative bias in the *y*-direction and a small positive bias in the *x*-direction will produce a constant resultant reaction force acting on the end mill, producing a slight deflection during the cutting process. In addition, this loading coupled with the geometry of the tool will result in increased chatter experienced by the tool as it rotates. This chatter not only affects the surface finish of the milled channel (Fig. 13), but will also drastically reduce the life of the end mill.

The uncoated tools frequently produce significant burring (Fig. 13a). For the cutting parameters used in this study there is burring on the top edges of the channel as well as a burr that obstructs half of the channel width and running the entire length. The top-edge burr results from a higher friction coefficient, adhesion, and a greater amount of heat generated during the cutting operation. Because of these factors, rubbing and plowing occur at the cutting edge, which pushes a significant amount of material in front of the tool and out of the channel instead of directing the material along the rake face and into the flutes. The coated tools do not produce any observable burring (Fig. 13b), suggesting that the cutting process is occurring at significantly lower temperature, with less friction and adhesion on the tool surfaces. This enables fracture at the chip root which creates a chip that can flow up along the flutes and removed from the cutting zone.

3.5. Tool integrity

As demonstrated above, diamond-coated WC end mills show significant improvement in both cutting performance and

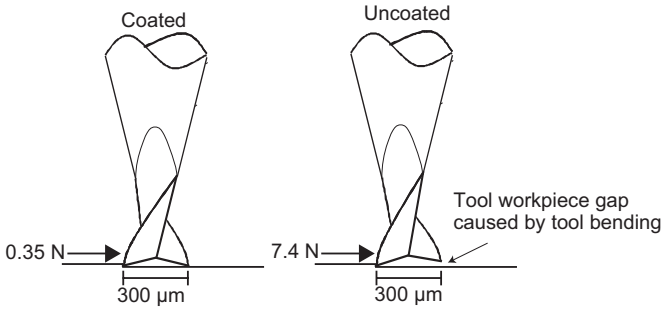

Fig. 14. Comparison of a coated and uncoated end mill during machining. The higher forces of the uncoated tool produce a deflection in the end mill causing for the retreating cutting edge to liftoff from the workpiece.

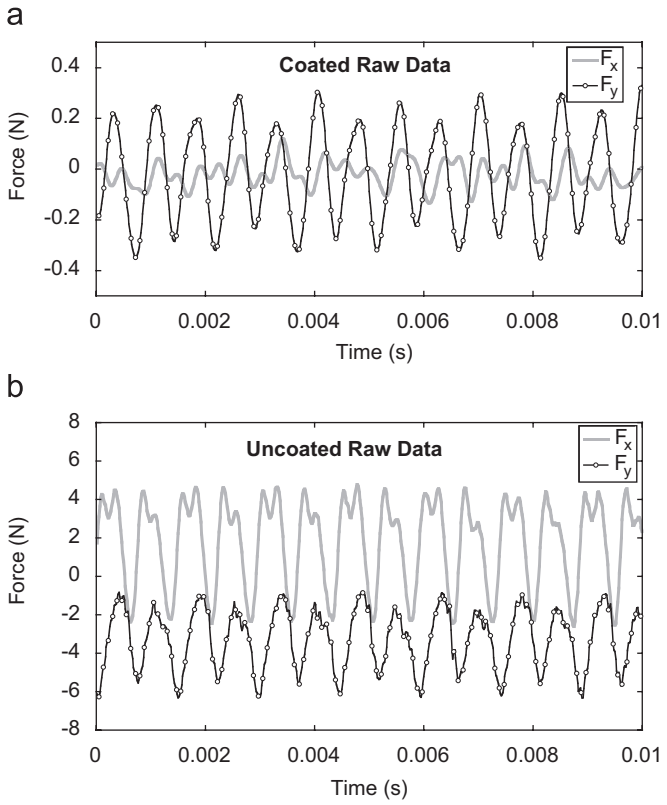

Fig. 15. Representative raw force measurements obtained during milling of (a) a coated end mill and (b) an uncoated end mill.

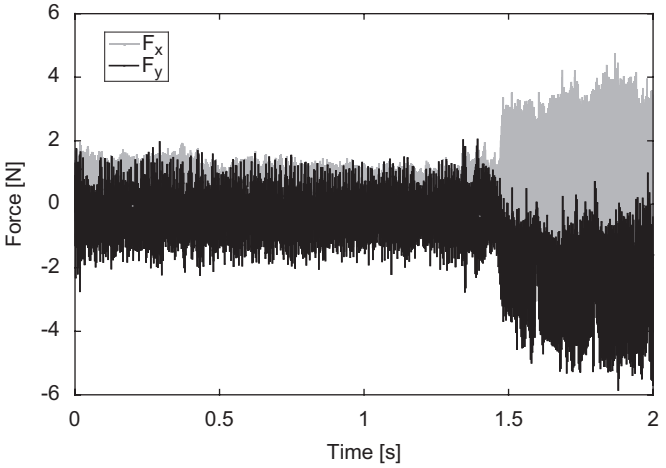

Fig. 16. Raw force measurements during delamination event of an FGD diamond-coated end mill.

workpiece surface finish when compared to bare WC end mills when dry machining aluminum. However, these performance gains are only experienced as long as the diamond coating survives. In several instances during testing, the diamond coating delaminated during milling. Upon delamination, tools with the thicker and larger grained FGD coating either return to a state of performance similar to an uncoated tool, or suddenly and catastrophically fail whereby the tool fractures. In either case, coating delamination occurs instantaneously with no measurable indication of coating failure beforehand. These coating failures are easily seen in the measured force data in which there is an abrupt increase in measured force (Fig. 16). In addition, there is an audible difference after coating failure. Typically, FGD-coated tools will produce very little to no audible noise during machining until the coating fails, while the excess forces and heat generated during the uncoated milling produce a rather distinct audible sound.

Further examination of the milled channel reveals a clear location where delamination of the FGD-coated tool occurs. The channel in Fig. 17a depicts such a scenario where the FGD-coated tool delaminated approximately halfway through the imaged section of the channel. Before delamination, the milled channel produced a clean, uniform channel with very little burring. After coating delamination, burring of the workpiece immediately began. In addition, the channel bottom produced a very sporadic surface topography. This happened in approximately 80% of the tests conducted under the conditions used in Table 2.

Coating delamination is also apparent upon further inspection of the failed FGD-coated end mills using an SEM (Fig. 17b). Large portions of the tool coating are fractured from the tool tips and cutting edges, and continue along the flank face of the end mill. Aluminum workpiece material has adhered to the underlying WC tool surface, resembling the tool condition and performance of the uncoated end mills tested previously. In several instances, the tool would catastrophically fracture immediately after coating delamination. The propagation of the delaminated coating throughout the tool suggests weak adhesion between the WC tool surface and the FGD coating.

The UDD-seeded tools with NCD coatings of approximately 200 nm thickness do show evidence of coating delamination, but without the same adverse effects seen with FGD-coated tools. Delamination of the UDD-seeded NCD-coated tools are restricted to only the high-stress areas at the cutting edge and do not propagate across the cutting tool surface. Tools would continue cutting after delamination with a slight increase in cutting forces. Eventually, continued delamination would result in tool fracture. This delamination was observed in approximately 40% of the tests conducted with the UDD-seeded NCD coatings. What is not known at this time is whether the denser UDD-seeding improves adhesion of the NCD coating to the WC substrate, or the thinner coating is not strong enough to break off large sections when local delamination occurs. Another possibility could be failure within the WC substrate which propagates to the surface and removes a small area of coating with it, meaning the event is tool fracture, not delamination, and will be generically referred to as "tool wear". Fig. 18 shows SEM images of coating delamination and WC wear along the flank edge. The type of WC wear that is seen here is not seen on bare WC tools cutting 6061-T6 aluminum, suggesting that the underlying WC structure failure may be the cause for this instance of delamination. The high wear areas along the flank face of the end mills have also experienced loss of the NCD coating (Fig. 18).

In addition, trace amounts of the aluminum workpiece had adhered to the surface of the NCD coating (Fig. 19), which was not present at all throughout the testing of the larger grained DET-seeded FGD coatings. Much of the adherent aluminum material appeared on the cutting tips of the end mills.

The cutting force traces do not provide clear evidence of when the tool wear event occurred (Fig. 20a). The peak magnitudes of the forces remain relatively constant throughout the machining test. Inspection of the workpiece channels after milling also produces the same inconclusive results (Fig. 20b). Therefore, the tool wear either occurred rapidly upon the tools' first contact with the workpiece, or resulted in very little change in the cutting forces. The delaminated NCD-coated tools produce a uniform workpiece surface finish with little indication of any smearing, but an observable amount of burring is apparent throughout the

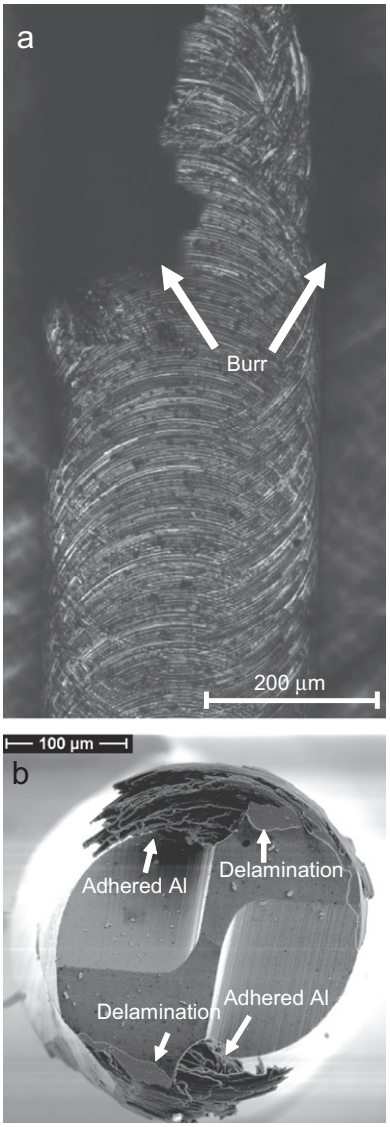

Fig. 17. (a) White light interferometric image of milled aluminum channel during FGD-coating delamination and (b) SEM image of delaminated FGD-coated micro end mill.

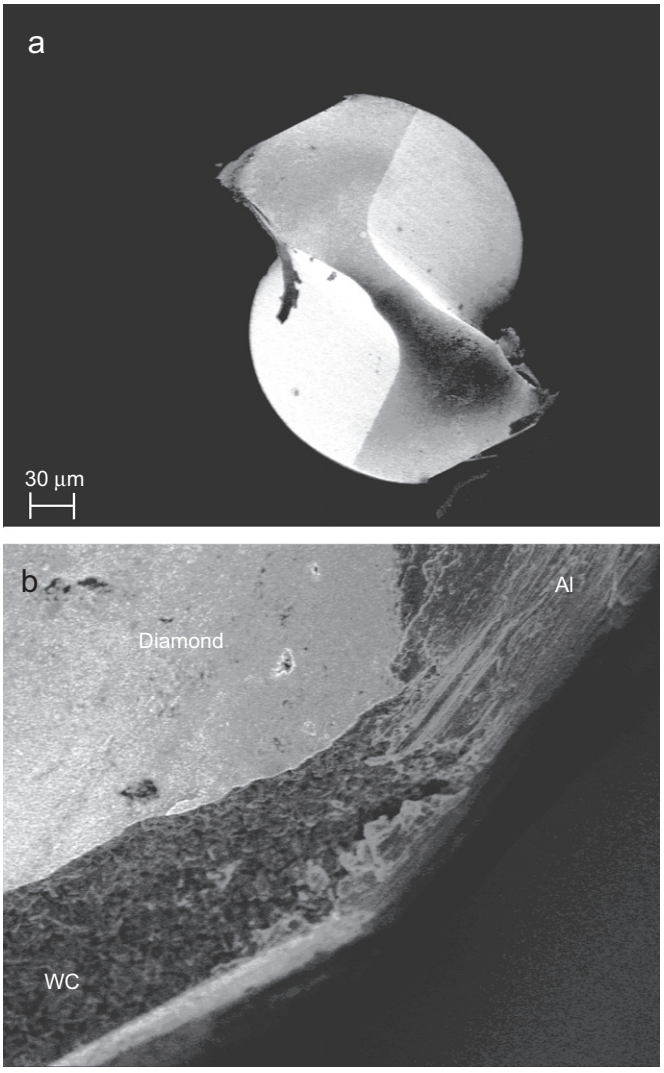

Fig. 18. SEM image of (a) delaminated UDD-seeded NCD-coated end mill and (b) worn flank face edge of end mill with areas of adherent aluminum

length of the cut. Overall, the amount of burring is not as considerable as the amount created by an uncoated end mill.

4. Conclusions

Nanocrystalline diamond films contain several favorable mechanical and tribological properties, such as a low coefficient of friction, high hardness, and chemical inertness particularly against aluminum. These coatings show great promise as a high-performance coating for micro-cutting tools. Proper tool preparation and HF-CVD film growth have led to continuous, uniform diamond coatings with thicknesses less than 600 nm. Using a solution-based diamond seed (UDD) resulted in a higher nucleation density and more consistent NCD coating thickness with an apparent grain size less than 100 nm and overall thickness less than 300 nm. Contrast to this, the dry, agglomerated detenation diamond seed (DET) produced FGD coatings that were approximately 600 nm thick with an apparent minimum grain size of 500 nm.

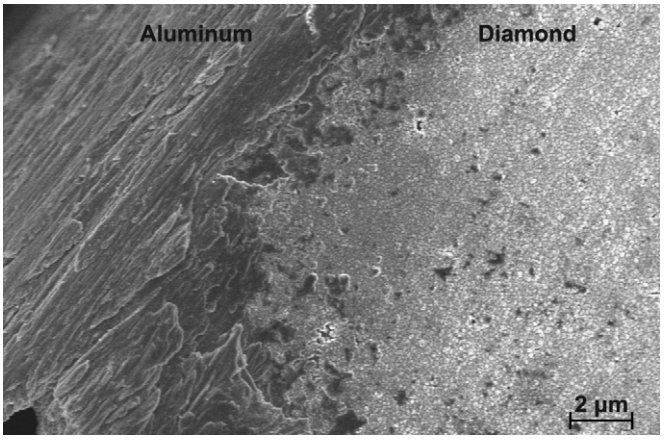

Fig. 19. SEM image of 6061-T6 aluminum workpiece material adhering to the UDD-seeded NCD-coated surface.

Force measurements during dry end milling have indicated a drastic increase in tool performance with approximately a 75% reduction in cutting forces and a 90% reduction in thrust forces

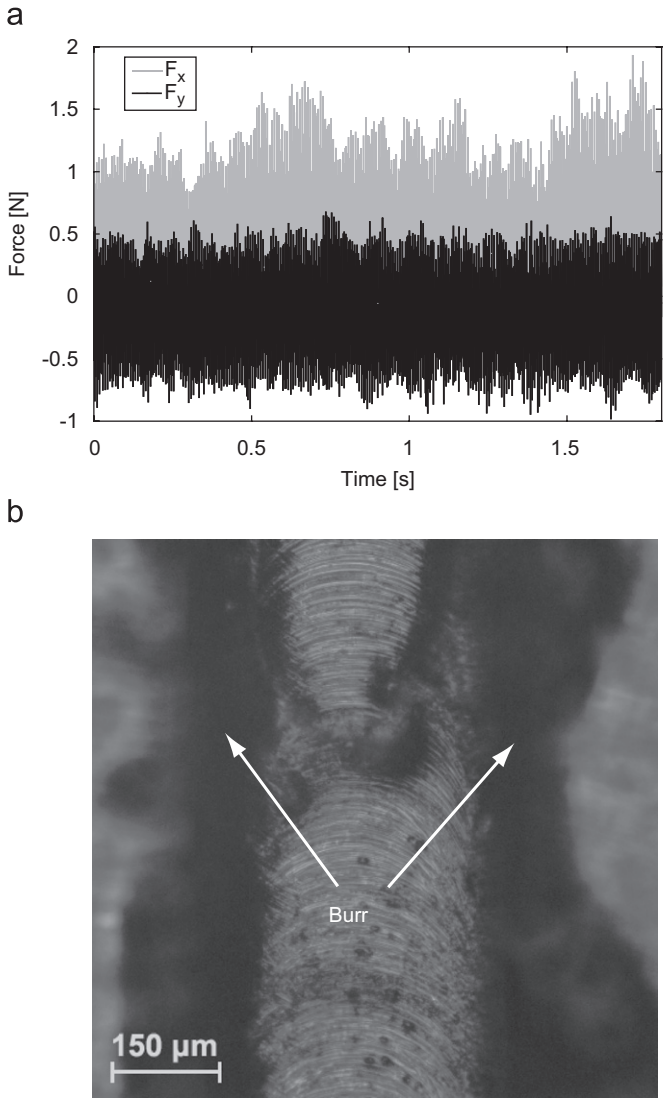

Fig. 20. (a) Measured raw force data from a delaminated UDD-seeded NCD-coated end mill and (b) white light interferometric image of milled aluminum channel from a delaminated UDD-seeded NCD-coated end mill.

when using the thicker, larger grained diamond coating. Using the thinner, UDD-seeded NCD coating produced a further reduction in cutting forces by approximately 50% compared to the DET-seeded FGD-coated tools. The sizeable performance increase can be largely attributed to the decrease in the frictional force and adhesion experienced by the cut chip sliding across the face of the tool. A smaller frictional force resulted in a larger shear angle within the primary deformation zone during the cutting process; resulting in thinner cut chip. Further analysis of the cut chips, tools, and channels after machining verified the performance gains of the coated tools.

Further investigation must be performed to increase the longevity of the NCD diamond coatings. In several instances, the FGD coating had completely delaminated form the WC tool surface, often resulting in catastrophic tool fracture. The UDD-seeded diamond coatings, on the other hand, did not produce such severe delamination results. In most cases, delamination was restricted to only locations of either high stress or high wear on the cutting tool and did not propagate throughout the tool. Unlike the FGD-coated end mills, the delamination of the UDD-seeded NCD-coated tools did not result in catastrophic tool failure.

Acknowledgements

Support of this research was initiated by funding from an Industrial and Economic Development Research Grant from the state of Wisconsin, and is now partially funded by NFS Grant CMMI-0700794/0700351, NSF-supported shared facilities, and the College of Engineering at the University of Wisconsin-Madison. Use of the Center for Nanoscale Materials was supported by the US Department of Energy, Office of Science, Office of Basic Energy Sciences, under Contract no. DE-AC02-06CH11357. The authors would like to thank David Burton of Performance Micro Tool for providing the micro end mills.

References

[1] F. Bruno, C. Friedrich, R.O. Warrington, The miniturization technologies: past, present, and future, IEEE Transactions on Industrial Electronics 42 (5) (1995) 423–430.
[2] R.E. Williams, Y. Huang, S. Melkote, B. Kinsey, W. Sun, D. Yao, Recent Advances in micro/meso-scale manufacturing processes, in: International Mechanical Engineering Congress and Exposition, Orlando, FL, November 5–11, 2005, pp. ICMECE2005-79889.
[3] J. Chae, S.S. Park, T. Freiheit, Investigation of micro-cutting operations, International Journal of Machine Tools and Manufacture 46 (3–4) (2006) 313–332.
[4] M.J. Jackson, G.M. Robinson, W. Ahmed, Micromachining selected metals using diamond coated cutting tools, International Journal of Nanomanufacturing 1 (2) (2006) 304–317.
[5] X. Liu, R.E. Devor, S.G. Kapoor, K.F. Ehmann, The mechanics of machining at the microscale: assessment of the current state of the science, ASME Journal of Manufacturing Science and Engineering 126 (2004) 666–678.
[6] M.J. Jackson, G.M. Robinson, M.P. Brady, W. Ahmed, Micromilling of bipolar fuel cell plates using titanium- and diamond-coated cutting tools, International Journal of Nanomanufacturing 1 (2) (2006) 290–303.
[7] A. Kobayashi, The features and application of UPC nano-micro forming tools, Industrial Diamond Review (2005) 28–30.
[8] B.N. Damazo, M.A. Davies, B.S. Dutterer, M.D. Kennedy, A Summary of micro-milling studies, in: First International Conference and General Meeting of the European Society of Precision Engineering and Nanotechnology, Bremen, May 31–June 4, 1999, pp. 322–325.
[9] C. Friedrich, P. Coane, J. Goettert, N. Gopinathin, Direct fabrication of deep X-ray lithography masks by micromechanical milling, Precision Engineering 22 (1998) 164–173.
[10] C.-J. Kim, M. Bono, J. Ni, Experimental Analysis of Chip Formation in Micro-Milling, Technical Paper Society of Manufacturing Engineers. MR MR02-159, 2002.
[11] K. Isomura, M. Murayama, H. Yamaguchi, N. Ijichi, N. Saji, O. Shiga, K. Takahashi, S. Tanaka, T. Genda, M. Esashi, Development of micro-turbo charger and micro-combustor as feasibility studies of three-dimensional gas turbine at micro-scale, In: ASME Turbo Expo 2003, Atlanta, GA, June 16–19, 2003, pp. 685–690.
[12] Y. Jeon, F.E. Pfefferkorn, Laser-assisted machining of silicon nitride with cubic boron nitride tipped micro end mill, in: Second International Conference on Micro-Manufacturing USA, Greenville, South Carolina, USA 2007, p. 43.
[13] M.B.G. Jun, R.E. Devor, S.G. Kapoor, Investigation of the dynamics of microend milling-Part II: Model validation and interpretation, Journal of Manufacturing Science and Engineering, Transactions of the ASME 128 (4) (2006) 901–912.
[14] M.J. Jackson, L.J. Hyde, W. Ahmed, H. Sein, R.P. Flaxman, Diamond-coated cutting tools for biomedical applications, Journal of Materials Engineering and Performance 13 (4) (2004) 421–430.
[15] H. Sein, W. Ahmed, M. Jackson, R. Woodwards, R. Polini, Performance and characterisation of CVD diamond coated, sintered diamond and WC-Co cutting tools for dental and micromachining applications, Thin Solid Films 447–448 (2004) 455–461.
[16] J. Gabler, L. Schafer, H. Westermann, Chemical vapour deposition diamond coated microtools for grinding, milling and drilling, Diamond and Related Materials 9 (2000) 921–924.
[17] C. Chang, Y. Liao, G.Z. Wang, Y.R. Ma, R.C. Fang, CVD diamond growth, in: Crystal Growth Technology, Springer, Heidelberg, 2003.
[18] M.J. Jackson, M.D.H. Gill, H. Sein, W. Ahmed, Manufacture of diamond-coated cutting tools for micromachining applications, Proceedings of IMechE Part L: Journal of Materials: Design and Applications 217 (1) (2003) 77–83.
[19] R.A. Hay, The new diamond technology and its application to cutting tools, in: Ceramic Cutting Tools, William Andrew Publishing/Noyes, Norwich, NY, 1994.
[20] J. Schwarz, K. Meteva, A. Grigat, A. Schubnov, S. Metev, F. Vollersten, Synthesis of diamond coatings on tungsten carbide with photon plasmatron, Diamond and Related Materials 14 (3–7) (2005) 302–307.

[21] H.Y. Ueng, C.T. Guo, Diamond-like carbon coatings on microdrill using an ECR-CVD system, Applied Surface Science 249 (1–4) (2005) 246–256.
[22] Y. Qi, E. Konca, A.T. Alpas, Atmospheric effects on the adhesion and friction between non-hydrogenated diamond-like carbon (DLC) coating and aluminum—a first principles investigation, Surface Science 600 (15) (2006) 2955–2965.
[23] J. Hu, Y.K. Chou, R.G. Thompson, J. Burgess, S. Street, Characterizations of nano-crystalline diamond coated cutting tools, Surface & Coatings Technology 202 (4–7) (2007) 1113–1117.
[24] I.P. Hayward, I.L. Singer, L.E. Seitzman, Effect of roughness on the friction of diamond on CVD diamond coatings, Wear 157 (2) (1992) 215–227.
[25] P.J. Heaney, A.V. Sumant, C.D. Torres, R.W. Carpick, F.E. Pfefferkorn, Diamond coatings for micro end mills: enabling the dry machining of aluminum at the micro-scale, Diamond and Related Materials 17 (3) (2008) 223–233.
[26] M.Y. Liao, X.M. Meng, X.T. Zhou, J.Q. Hu, Z.G. Wang, Nanodiamond formation by hot-filament chemical vapor deposition on carbon ions bombarded Si, Journal of Crystal Growth 236 (1–3) (2002) 85–89.
[27] J.E. Butler, H. Windischmann, Developments in CVD-diamond synthesis during the past decade, MRS Bulletin 23 (9) (1998) 22–27.
[28] F.G. Celii, J.E. Butler, Diamond chemical vapor deposition, Naval Research Reviews 44 (3) (1992) 23–44.
[29] O.A. Williams, M. Nesladek, Growth and properties of nanocrystalline diamond films, Physica Status Solidi A 203 (13) (2006) 3375–3386.
[30] G. Boothroyd, W.A. Knight, Fundamentals of Machining and Machine Tools, CRC Press, Boca Raton, FL, 2006.
[31] M.C. Shaw, Metal Cutting Principals, Oxford University Press, New York, 1984.
[32] A. Erdemir, G.R. Fenske, A.R. Krauss, D.M. Gruen, T. Mccauley, R.T. Csencsits, Tribological properties of nanocrystalline diamond films, Surface and Coatings Technology 120–121 (1999) 565.